CHAPTER 3: RESULT AND DISCUSSION

3.1 Electrodepositon Cu-Pb Alloys from MSA Bath

From this study, electrodeposition Cu-Pb alloys from a Methane Sulfonic Acid (MSA) bath with copper (II) acetate monohydrate as a copper source and lead acetate trihydrate as a lead source can be represented following equation in Table 3.1 with the intermediates during the electrodeposition process. The second side reaction in addition to the hydrogen ion reduction is referred to the reduction of water.

Table 3.1: Reduction reaction during the Cu-Pb alloy deposition from MSA bath

No	Reactions
1	$Cu^{2+} + e^- \longrightarrow Cu^+_{ad}$
2	$Cu^+_{ad} + e^- \longrightarrow Cu$
3	$Pb^{2+} + e^- \longrightarrow Pb^+_{ad}$
4	$Pb^+_{ad} + e^- \longrightarrow Pb$
5	$H^+ + e^- \longrightarrow H_{ad}$
6	$H_{ad} + H^+ + e^- \longrightarrow H_2$
7	$2H_2O + 2e^- \longrightarrow H_2 + 2OH^-$

The Cu-Pb alloy electrodeposition was performed on the same size of steel plates which was described in the previous section (Chapter 2). Electrodeposition of Cu-Pb alloy was carried out from the MSA bath for 45 min when the operating conditions were set as (Section 2.2). In all experiments the electrolyte contained constant concentration of the following components (mole/dm^3): Pb^{2+} - 0.30, Cu^{2+} - 0.10 and CH_3SO_3H (free) - 1.00 (100 g/dm^3). The metal electrodeposition process from an aqueous bath is affected by the hydrogen evolution reaction (HER) and influences the morphology of the electrodeposited surface. The electrodeposition of Cu-Pb at different current density will be discussed.

The Cu^{2+} is nobler ($E_{\circ}$= +0.34 V) compared to Pb^{2+} ($E_{\circ}$= -0.13 V) that the divalent lead ions are reduced to Pb in the two steps as shown in the following reactions:

$Pb^{2+} + e^{-} \rightarrow Pb^{+}$ Fast ..... (3.1)

$Pb^{+} + e^{-} \rightarrow Pb$ Slow ..... (3.2)

According to reaction (3.1) and (3.2), during the electrodeposition process accumulation of Pb^{+} species appears on the surface of steel. EDX result of the chosen samples show that Pb content is enhanced in the deposit layer that were derived from MSA bath with increased current densities.

3.2 Physical Appearances of Quiescent Bath At a room temperature

Table 3.2 show the physical appearance of Cu-Pb electrodeposits at various current densities for a quiescent MSA bath at room temperature. The Cu-Pb alloy were deposited from a solution containing 0.3 mol dm^{-3} Pb(II) + 0.1mol dm^{-3} Cu(II) + 1.0 mol dm^{-3} methane sulfonic acid using a current density of 4 mA cm^{-2} to 18 mA cm^{-2} at room temperature. The observation of the surfaces of copper-lead deposits did not reveal much concerning its electrocrystallization.

At 4 mA cm^{-2} and 6 mA cm^{-2} freshly deposit material, the electrodeposit had very brownish appearances, smooth and a bit bright were obtained (Figure 3.1). Both of electrodeposit showed good ductility and had good adhesion since no flaking or cracking were observed when the deposits were bent with the steel substrate. From 8 mA cm^{-2} to 10 mA cm^{-2}, electrodeposits which were semi-bright, semi-smooth and having a dark brownish and black appearance were observed. The deposits had a matt and a slightly rough appearance; the optical reflectivity of the surface was poor compared to the steel substrate. Some peeling of the alloy from the substrate was observed when the deposit was bent with the steel substrate. Electrodeposits obtained at current densities of around 12 mA cm^{-2} and above, the characteristic had a brittle black, not smooth and were quite dull. Deposits obtained within the current density range of

about of 12 mA cm^{-2} or more had a coarse surface texture and its surface looked a bit powdery and rough. The darkness of the electrodeposits increase as the current density was raised from range of 4 mA cm^{-2} to 18 mA cm^{-2} without additive in the electrolyte. Moreover, by observing the deposit visually it is noticed that the formation is more homogeneous coating over the substrate's surface.

Table 3.2 Quiescent MSA bath at a room temperature

Current Density mA/cm^2	Description of Electrodeposition Copper-Lead Alloys
4	Light brownish, uniform, bright, smooth (but not glossy)
6	Light brownish, uniform, bit bright, smooth
8	Black and dark brownish, not bright, bit dull, uniform, semi-smooth
10	Black and dark brownish, uniform, quite dull, semi-smooth
12	Black, compact, not smooth, quite brittle too
18	Brittle black, compact, not smooth, bit powdery

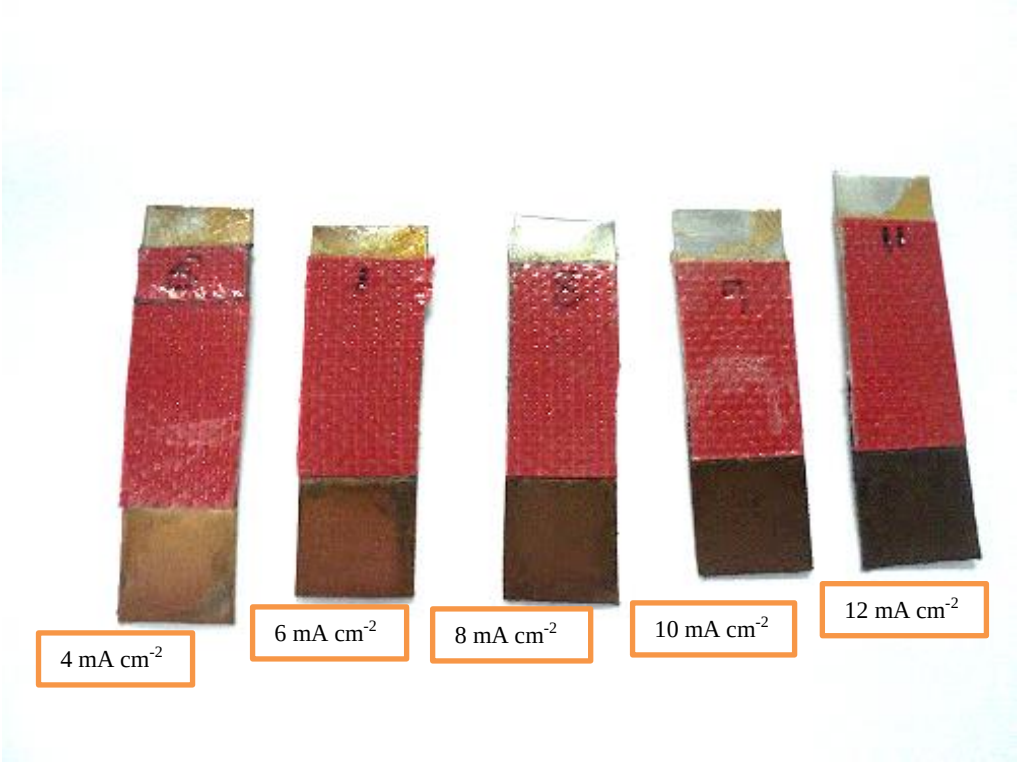

Figure 3.1 Electrodeposits sample at different current densities.

3.3 Mass Electrodeposition

This section investigates the mass electrodeposition of Cu-Pb alloys electrodeposited from solution containing 0.3 mol dm^{-3} Pb(II) + 0.1mol dm^{-3} Cu(II) + 1.0 mol dm^{-3} methanesulfonic acid. The movement of ions can be enhanced with increasing the current density to the electrode surface from the bulk solution. Consequently, the mass of the electrodeposition is increased with the increased of current density that is reported by numerous researchers. The electrodeposition was performed in the presence of MSA. As earlier mentioned, the Multichannel Potentiostat / Galvanostat WMPG5000 was used to generate the proper current density. The massogram (Figure 3.2) shows that the mass deposition for a range of current densities. The mass of Cu-Pb alloy electrodeposited layers were determined from difference of mass before and after the electrodeposition of steel plates measurement in the micro-balance scale (Table 3.3). Obviously, the difference between the mass electrodeposited was enhanced with the increase of current density. Thematically, the Lorentz force (F_L) is greater in the higher current density, thus it gave the more mass depositing at the higher current densities (4.0 to 18.0 mA cm^{-2}) as it can see in Figure 3.2.

Table 3.3 Mass of electrodeposition at different current densities.

Sample	Current Density mA cm^{-2}	mass of steel panel before alloy electrodeposition A, g	mass of steel panel after alloy electrodeposition B,g	Average B-A, g
1	4	1.0958	1.0993	0.0035
2	6	0.9742	0.9796	0.0054
3	8	0.9482	0.9553	0.0071
4	10	0.9634	0.9716	0.0082
5	12	1.0579	1.0691	0.0112
6	18	0.9837	1.0006	0.0169

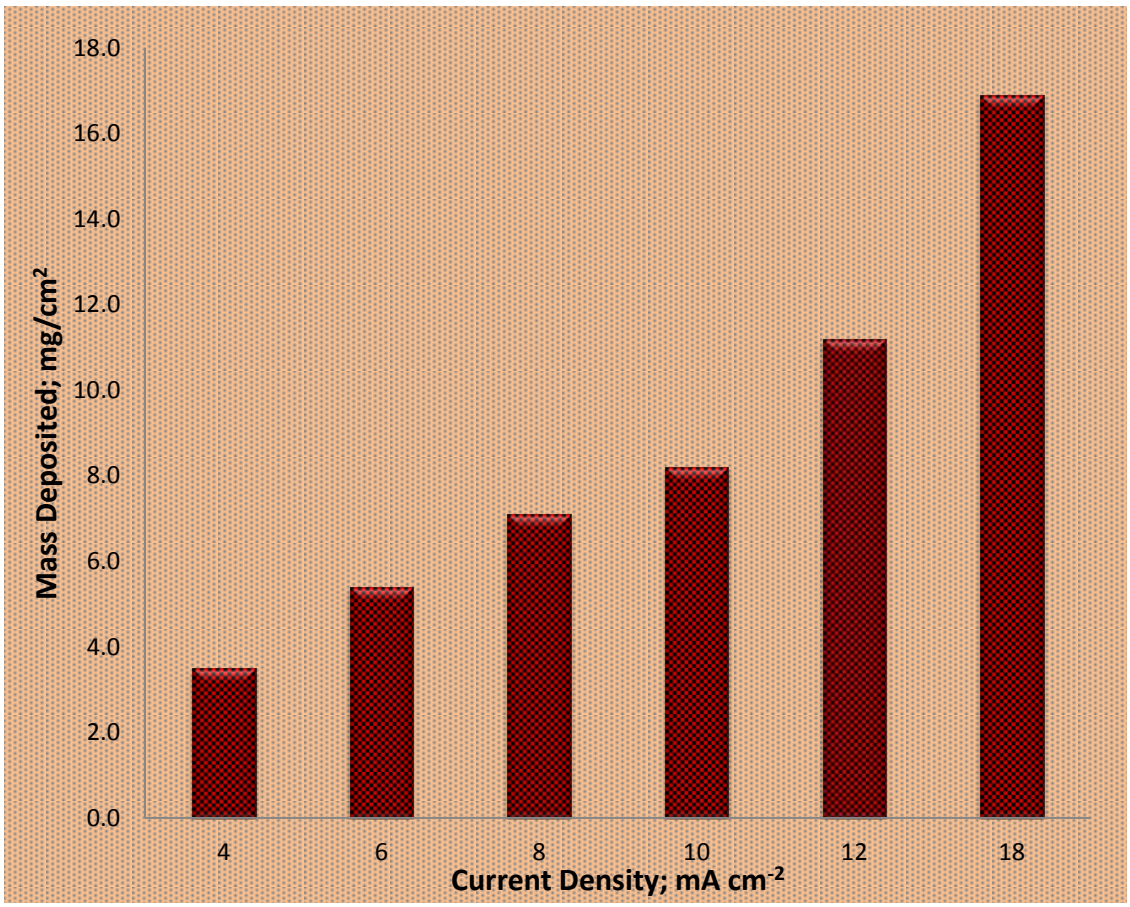

Figure 3.2 The mass deposition of Cu-Pb alloy at different current densities in MSA bath for 45 min.

3.4 Current Efficiency

The current efficiency is defined as the proportion (in percentage) of the total current used for the cathodic deposition or anodic dissolution of metal or alloy (A.Brenner, 1963). It is stated in Faraday's laws that the amount of chemical charge at an electrode is exactly proportional to the total quantity of electricity consumed. However, if several reactions take place simultaneously at the electrode, side reactions may consume the product. Therefore, inefficiencies may arise from the side reactions other than the intended reaction taking place at the electrodes. Current efficiency is a fraction, usually expressed as a percentage, of the current passing through an electrolytic cell (or an electrode) that accomplishes the desired chemical reaction. Or,

Current efficiency = $100 \times W_{Act} / W_{Theo}$ …… (3.3)

where W_{Act} is the weight of metal deposited or dissolved, and W_{Theo} is the corresponding weight to be expected from Faraday's laws [Eq. (3.3)] if there is no side reaction. Note that the cathode efficiency is the current efficiency applied to the cathode reaction and the anode efficiency is the current efficiency applied to the anode reaction. The efficiencies are not always 100% as hydrogen and oxygen are simultaneous evolved at the cathode and the anode respectively.

The current efficiency for Cu-Pb electrodeposition can be calculated from the Faraday's law where,

$$\emptyset = \frac{mnF}{tAjM} = \left(\frac{m}{tA}\right)\left(\frac{nF}{jM}\right) \quad \text{..... (3.4)}$$

Where m = the mass of electrodeposition / g, t = is the electrodeposition time / s, A = surface area of deposition / m^2, n = number of electron involved in reduction of copper and lead ions, F = Faraday constant / $Cmol^{-1}$, j = current density / A m^{-2}, M = average molar mass of copper and lead is 135.35 g mol^{-1} and Ø is the electrodeposition efficiency, $\left(\frac{m}{tA}\right)$ is also the mass electrodeposition rate.

Table 3.4 shows the mass electrodeposition efficiency was calculated and the HER percentage was tabulated. From Figure 3.4, it can be seen that electrodeposition of Cu-Pb alloys have higher current efficiencies for various current density in MSA bath. The hydrogen Evolution Reaction (HER) increase was small compared to the increase of metal electrodeposition on the electrode surface. In mildly acidic solution, the HER can arises from these reaction at the cathode:

$$2H^+ (aq) + 2e^- \longrightarrow H_2 (g) \quad \text{..... (3.5)}$$

$$2H_2O (l) + 2e^- \longrightarrow H_2 (g) + 2OH^- (aq) \quad \text{..... (3.6)}$$

Electrodeposition of Cu-Pb is much enhanced compared to the HER because some of the HER comes from the water molecules which do not carry charges, so the water molecule doesn't experience Lorentz force. The proton carries a single charge which

experiences a smaller Lorentz compared to the Lorentz force experienced by the copper and lead ions which both are double charged ions.

Theoretically, electrodeposition at higher current density will decrease the current efficiency due to hydrogen evolution. However, Cu-Pb alloys electrodeposition via MSA has shown excellent current efficiency which is as high as 99.2%. Based on the result in Table 3.4, the average current efficiency was 94.2% when electrodeposited with Cu-Pb alloys using current density of 4 mA cm^{-2} to 18 mA cm^{-2} at room temperature. However, there was a sudden drop for current efficiency when deposited at 10 mA cm^{-2} current density. The ion H^+ from acid was reduced to hydrogen gas during electrodeposition. The hydrogen gas was co-deposited onto the steel substrate, thus causing the Cu-Pb alloy deposit was dull, porous and had poor reflectivity as shown in Figure 3.1.

Table 3.4 Gives the electrodeposition efficiency with different current density in MSA bath.

Current Density mA cm^{-2}	Δm(mg cm^{-2})	Efficiency %	HER %
4	3.5	92.4	7.4
6	5.4	95.1	4.9
8	7.1	93.7	6.3
10	8.2	86.6	3.4
12	11.2	98.6	1.4
18	16.9	99.2	0.8

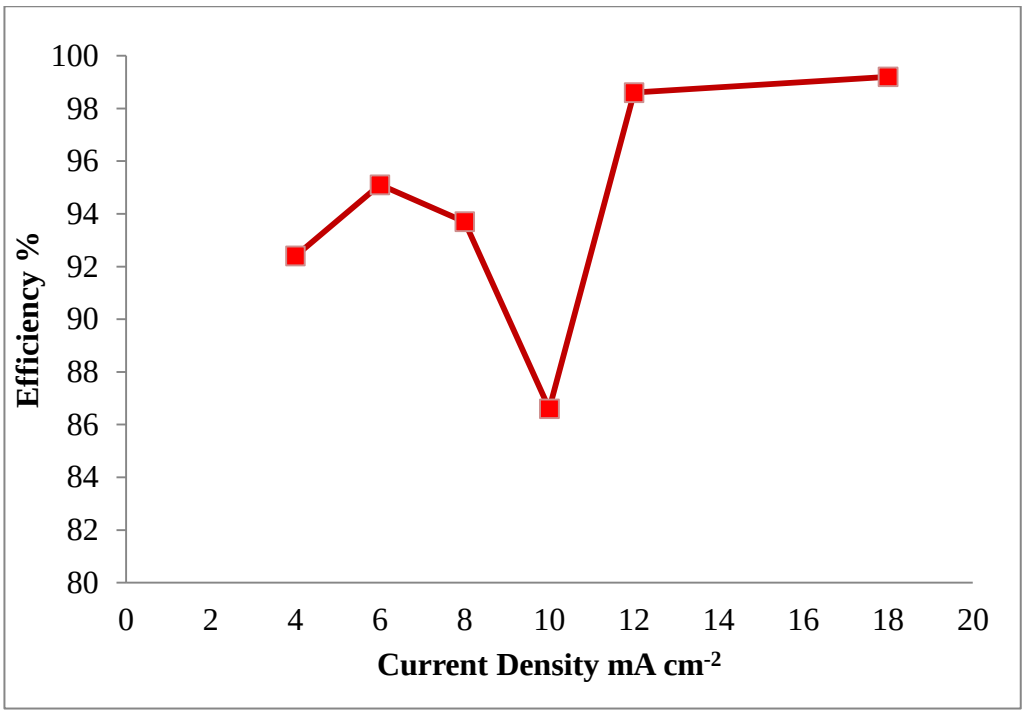

Figure 3.3 Variation of current efficiency with deposition current density

The current efficiency, Q_{eff} = n is defined as the proportion (in percentage) of the total current used for the cathodic deposition or anodic dissolution of metal or alloy (Brenner, 1963; Raub, 1967).

The cathode current efficiency measures the effective utilization of electrical energy and thus is important. A knowledge of the cathode current efficiency will enable us to determine the deposits thickness and hence the output of product from an operation. The cathode current efficiency and alloy composition curve can provide us with some information as to how plating variables affect alloy composition.

In alloy composition where hydrogen evolution occurs, the variation in current efficiencies of each metal involved may be independent of each other at the expense of the efficiency of hydrogen discharge. For alloy deposition with current efficiency of 100%, then the variation of the efficiencies of each of the two metals are dependent on each other; as a decrease in one an increase in the other.

Brenner (1963) indicated that there were two general cases involving variation in efficiency of alloy deposition. Firstly, when there is no change in the composition of

the alloy it indicates that the current efficiency of the deposition of the metal has increased or decreased in the same proportion. Secondly, when there is a change in the alloy's composition it indicates that the current efficiencies of deposition of each metal have changed unequally; they may have changed in the same time sense, opposite or one may have been constant.

3.5 X-ray Diffraction

All six electro-coated samples and uncoated steel substrate were chosen for the XRD analysis, which is shown in Fig. 3.4 (a-g). The evolution and formation of the deposits coating at each deposition current density were examined. The XRD diffraction peaks of deposited layer were procured from the scan range of 2θ values from 5º to 80º to observe the phase, structure and crystallite size of the samples. Figure 3.4 (a) show the XRD pattern of uncoated steel which it is clearly observed from sharp peak appearing at 44.5º with relative intensity of 100% can be attributed to the (110) plane of Iron, while peak at 64.8º correspond to the (200) plane Iron, respectively. The XRD pattern is much similar to that ICDD standard iron metal (PDF 00-006-0696). In the X-ray pattern of the deposits of Cu-Pb alloy in Figure 3.4 (b -g) peaks can be identified that correspond to the Cu and Pb phases and their intensities vary as a function of the current densities in the coating. The identification of the crystallographic structure was performed by comparison with the reference diffraction pattern of standard copper metal (PDF 01-070-3038) and standard lead metal (PDF 00-000-0686). The indicated phases are matched with the phases obtained from database pattern. As result, the XRD patterns show that the coatings consist of a mixture of crystals of the two metals irrespective of current density used. These results agree well with those obtained previously whether the deposits were obtained from simple salt bath or from baths containing the metal as complex ions (Brenner, 1963). Agglomeration of the two metals into separate phases is likely because the solubility of Pb in Cu and Cu in Pb is less than 0.01% at room temperature (Brenner, 1963). Even for electroplated Cu-Pb alloys, separate peaks for copper and lead were observed in the diffractogram indicating that copper and lead are electroplated next to each other as expected. For the alloy, reflections for both copper and lead are observed showing that

the metals are deposited side by side on the surface. Therefore at the deposition of the Cu-Pb coating whereas methanesulfonate electrolyte without organic additives with current density of 4 –18 mA cm^{-2} the alloy is formed of the kind of mechanical blend of the crystals. The deposition of the alloy according to the mechanism of the separate nucleation of metals each component of the alloy is usually deposited on its own substrate i.e., the process of the discharge of the ions of each metal runs not on the overall surface but on a portion thereof equal to the volumetric portion of this metal in the alloy (Gamburg, 1997).

According to the XRD pattern as shown in Figure 3.4 (b-g), the diffraction peaks of the copper and lead alloy show considerable broadening. This was an indication of very fine crystallite size in coating. All the reflection patterns for these samples indicated that the coatings are having a face centered cubic (FCC) structure. For the copper, three predominant peaks had been found which were at (111), (200) and (220) planes. On the contrary, the lead lines peak are corresponded to (111), (200), (222), (311) and (220) planes which controlled by current densities. The four reflections observed at 43.1º, 50.3º, 65.2º and 73.8º are consistent with a Cu-Pb alloys phase. From Table 3.5, the intensity of planes (111, 200) of copper reduced with increased of current density. The reverse effect was observed for the peak with plane (111, 200) of lead where the intensity increased with the increased of current density for electrodeposition of the Cu-Pb alloys. Changes in the intensity of the characterisation diffraction peaks of each phase with the change of current densities parameter. This indicates that the Cu-Pb crystals are oriented preferentially with their basal plane parallel to the steel surface. There was an iron peak observed in these patterns (brown line) which from steel substrate, however the relatively intensity and peaks counts is very much low compared to uncoated steel substrate (Figure 3.4(a-g)). The XRD figures illustrates that textures (220) were diminished and the texture (200) and (111) were enhanced in the increasing

of current density. The scale factor of the copper – lead alloy coating depends on the deposition current densities used during preparation. However, the detection of lead lattice at low current density (4 to 6 mA cm^{-2}) cannot be proven very clear by XRD result. So the EDX was used to detect the lead in the deposit alloys.

Table 3.5 XRD intensities of Cu-Pb alloy via different applied current densities

current Density mA/cm^2	**Intensity of peaks Cu**			**Intensity of peaks Pb**				
	111	**200**	**220**	**111**	**200**	**222**	**311**	**220**
4	80842	19809	17801			5824		
6	67845	17795	19944		136	4936		
8	42875	9611	4773	987	276	2426		
10	28680	5833	2743	1965	1051	2653		
12	21320	4411	2445	4479	944	1414		
18	12345	2700	1559	5964	1183	881	789	1134

Also reported in the Table 3.6 is the mean grain size which was estimated from the width of the strongest diffraction peak using the Debye –Schrerer equation. The grain size changing of deposited layers were calculated from XRD data through the Debye–Scherrer equation (Cullity and Stock, 2001); as shown in equation (3.7)

$$\gamma = \frac{0.9\,\lambda}{FWHM\cos\theta} \quad \text{..... (3.7)}$$

where λ = 1·540 Å is the wavelength, FWHM is the Full Width at Half Maximum (in radians), γ is the grain size/nm and θ is the angle satisfying Bragg's law.

Table 3.6 XRD Analysis of electrodeposited Cu-Pb obtained at different applied current densities.

Current density $mAcm^{-2}$ ↓	Character			Grain Size (nm)				
	Cu			Pb				
	111	200	222	111	200	222	311	220
4	33.4	21.4	27.7			73.5		
6	30.3	20.2	24.3		10.2	100.5		
8	25.7	14.3	17.7	9.0	10.2	36.8		
10	23.8	13.2	14.9	10.1	13.6	30.6		
12	27.8	14.3	12.1	11.5	20.4	36.8		
18	27.8	12.3	12.2	40.3	108.5	73.7	30.2	43.2

The crystallite size of the copper-lead alloy coating were calculated using the clearly separated peak after correction of the instrumental broadening of the (111) plane. The shape of the diffraction peaks indicates that the samples are well crystallized. The mean crystallite size of the copper-lead alloy coating is dependent on the deposition current density. It can be concluded that the crystallite size of the copper-lead alloy coating increases by increasing the deposition current density. The mean crystallite size of the Cu and Pb deposited at the deposition current density from 4 to 18 mA cm^{-2} which is estimated according to the Debye–Scherrer equation are 28.1 nm and 17.7 nm, respectively. Table 3.6 shows the grain size of copper peaks (111, 200) decrease with increase of the current density. Meanwhile grain size of lead coated layers on (111, 200) increasing with increase of current density from 4 to 18 mA cm^{-2}. However the determination grain size and strain of electrodeposition layers could not easily calculated with Debye-Scherrer equation because the estimation of grain size and strain of alloys with XRD data is complex (Ganesh, et al. 2005).It is depended to fraction on compound in alloys.

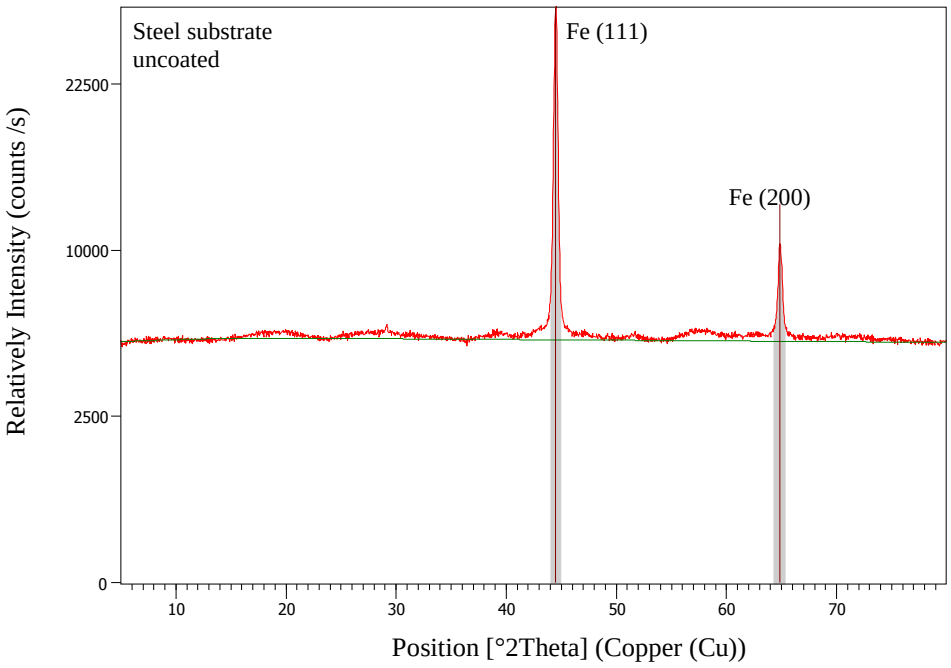

Figure 3.4 (a): X-ray diffraction pattern of the steel substrate before electroplating experiment

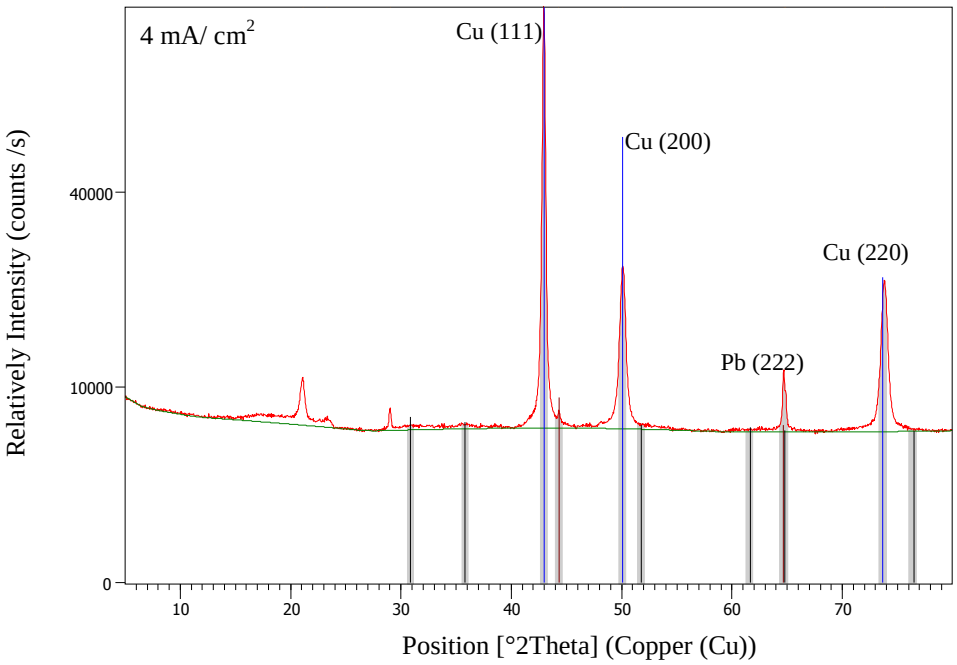

Figure 3.4 (b): X-ray diffraction pattern of the electrodeposited Cu-Pb alloy on steel substrate obtained at 4 mA cm^{-2}.

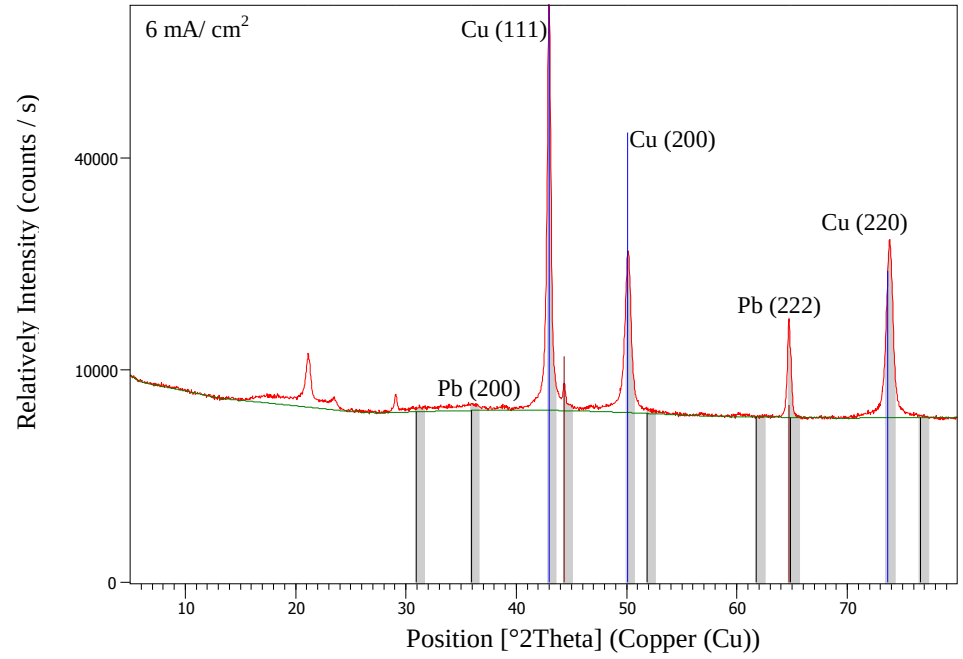

Figure 3.4 (c): X-ray diffraction pattern of the electrodeposited Cu-Pb alloy on steel substrate obtained at 6mA cm^{-2}.

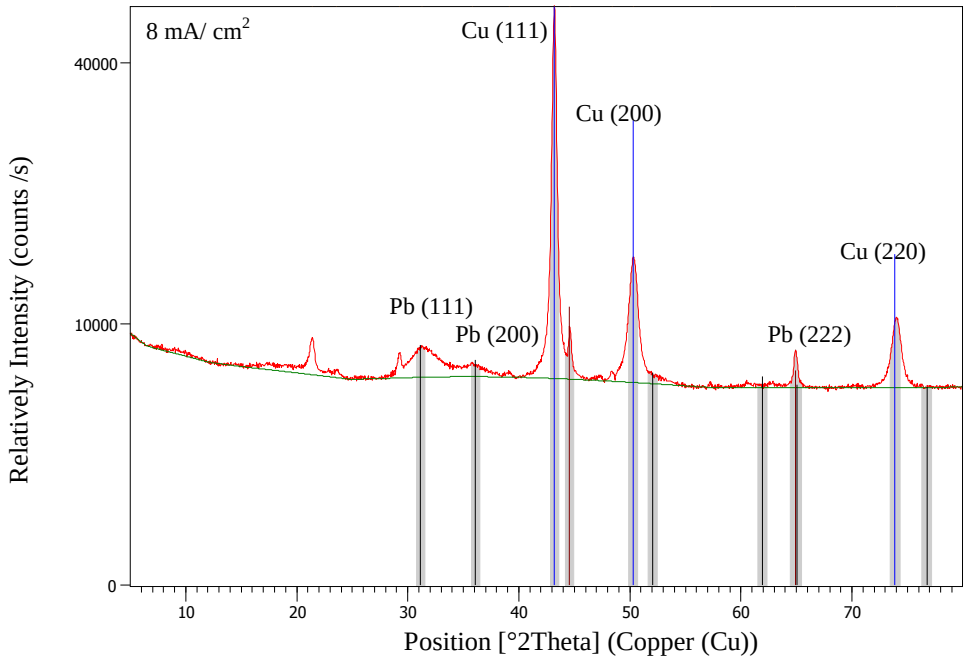

Figure 3.4 (d): X-ray diffraction pattern of the electrodeposited Cu-Pb alloy on steel substrate obtained at 8 mA cm^{-2}.

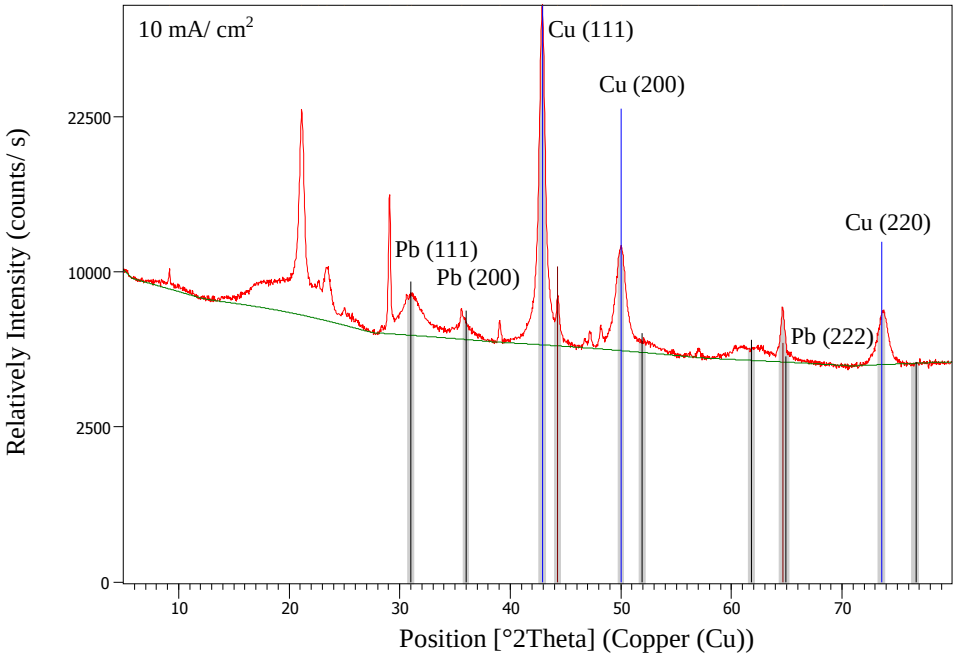

Figure 3.4 (e): X-ray diffraction pattern of the electrodeposited Cu-Pb alloy on steel substrate obtained at 10 mA cm^{-2}.

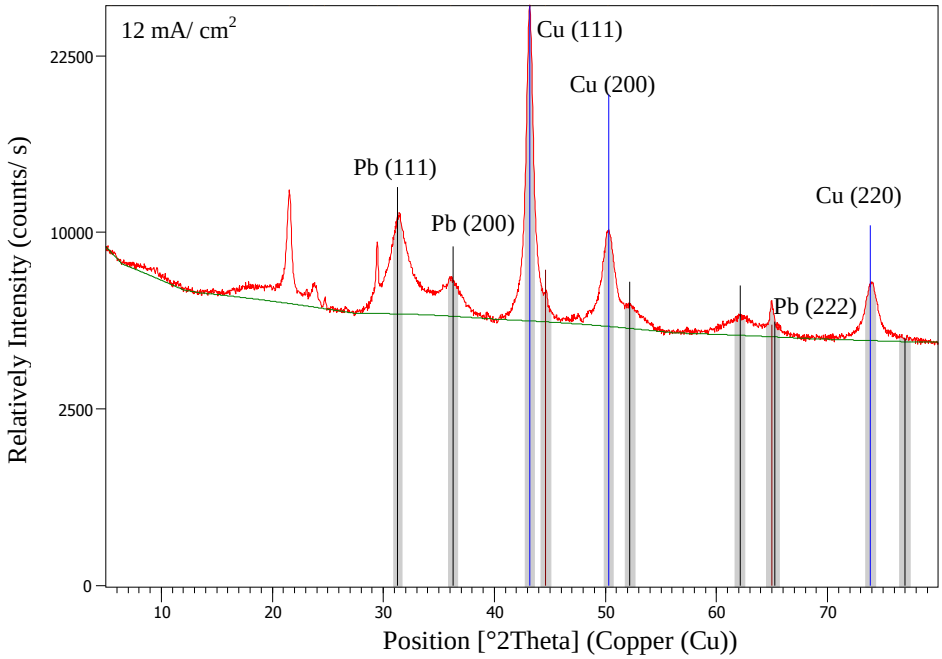

Figure 3.4 (f): X-ray diffraction pattern of the electrodeposited Cu-Pb alloy on steel substrate obtained at 12 mA cm^{-2}.

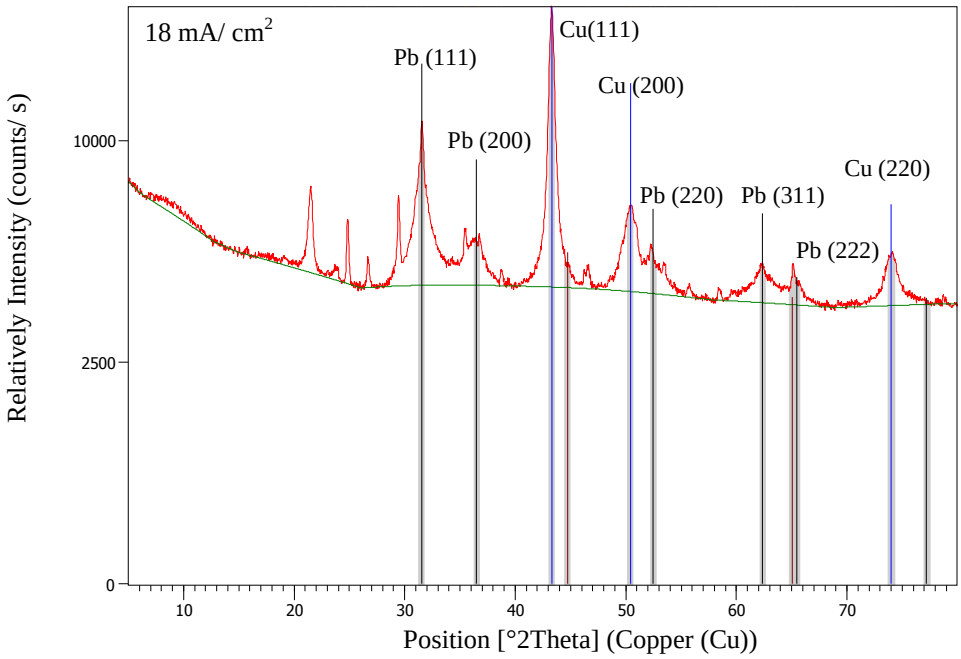

Figure 3.4 (g): X-ray diffraction pattern of the electrodeposited Cu-Pb alloy on steel substrate obtained at 18 mA cm^{-2}.

3.6 Scanning Electron Microscopy / Energy Dispersive X-ray (SEM/ EDX) analysis

The surface morphology of the Cu-Pb electrodeposited layer obtained from MSA bath was investigated via Scanning Electron Microscopy (SEM). Figure 3.6- 3.9 (a-f) shows SEM images of the surface microstructure of Cu-Pb alloys with a magnification of 500, 1000, 2500 and 5000 times at 20kV. A careful microscopic examination of alloy deposits may reveal some interesting information regards their microstructure in some cases. The EDX spectrum in the Figures 3.10 (a) through (f) corresponds to the SEM images (magnification 2500 times) in the Figures 3.8 (a) through (f) analyzed under 20 KeV. The elemental component in each sample was obtained using EDX, were tabulated in Table 3.7. From EDX analysis, it was discovered that the electrodeposition of lead was enhanced compared to copper despite concentration. Nevertheless, SEM / EDX analysis confirmed the Cu-Pb alloy deposition onto a steel substrate.

In addition, Figure 3.5 (a-d) are shown SEMs of uncoated steel substrate at different magnification whereas can be seen the images found to be plain and flat. Thus, EDX spectrum clearly observed that only element iron consist in the steel substrate. This was confirmed by the XRD data (Figure 3.4 (a)). The SEM images (Figures 3.6 – 3.9 (a-f)) are layers that were electrodeposited at current densities ranges of 4 mA cm^{-2} to 18 mA cm^{-2} for 45 min at room temperature respectively, in mixture of Cu^{2+}, Pb^{2+} and MSA. In this case, the images layer electrodeposited without presence of the additive in the MSA electrolyte. The general morphological trends occurred when varying the current density can be observed in these images. As can be seen from (Figures 3.6 – 3.9 (a-f)) that morphology of electrodeposit is quiet uniformed and adherent. The surface characteristics of deposits obtained at current densities of 4 mA cm^{-2} to 18 mA cm^{-2} were quite similar when seen under the microscope: they have a coarse sand appearance. Although the surface appeared smooth visually it resembled coarse sand under the microscope. It is discovered the morphology of the Cu-Pb alloys generally detected in dendrite particles and different type of agglomerates particles of size varying from about 5 to 200 µm. These agglomerates are characterized with the presence like nodular and well defined cauliflower feature in the micron scale. At 5000 times magnification (Figure 3.9(a-f)) shows the morphology of Cu-Pb is nearly rounded grain and cauliflower shapes obtained from electrodeposition. As can be seen (Figure 3.6 (a-f)) at low current density (4 – 6 mA cm^{-2}) the deposits is mostly nodules-like which is characteristic of Cu electrodeposited near the limiting current density. The nodular structure appeared to have quite large grain and some cauliflower crystallites when it was deposited at current densities of 8 to 10 mA cm^{-2}. At current densities of approximately 12 mA cm^{-2} or above, the electrodeposits were loose and contain dendritic shaped grains in nature. Although the coating obtained from the electrolyte solution was uniform but it quiet strongly adhere on the surface of substrate. The

formation of such dendritic shaped grains probably arises as a consequence of hydrogen gas bubbles clinging to the growth grain (Raub, et al. 1950).An increased mass transport of lead ions have diminished the effect of hydrogen evolution which gave larger lead crystallites, prevented the appearance of holes attributed to hydrogen evolution and gave more dense lead deposits. These features were found to be dependent on the condition of electrodeposition. In fact, Raub et al. (1976) mentioned that the growth of deposits may be dependent on the depositing condition. The alloy layer exhibited rougher morphology than a plated steel plate. From the SEM images, it can be seen that the electrodeposited brightener surface decrease as current density increased. Increasing Pb content of the deposit effects their smoothness and brightness. Montoro reported that the deposit brittleness is caused by migration and agglomeration of Pb at room temperature, leaving the Cu crystal with no binding material between them. Worthy of note is the fact that the morphologies of Cu-Pb alloy layer electrodeposited from MSA bath are different. It is important to point out that codeposited lead has a profound grain refining effect. As the lead content increases, the crystallite size also increases (Figure 3.6).

At larger magnification it can be seen that free steel surface is available between the crystals. Iron deposit was also observed on the surface layer confirmed through the EDX spectrum (Figure 3.10 (a-f)). It is marked on the SEM images as red arrow shown on SEMs Figure (3.7-3.9 (a-f)). Besides, there are some minor contaminants which have contributed during the eletrodeposition Cu-Pb plating process. The contaminant found to be co-deposited with Cu-Pb on steel substrate (EDX spectrum, Figure 3.10 (a-f)). This contaminant such as O only present in a very minor amount, therefore the result of the amount of Cu and Pb co-deposited on the steel substrate were not much effect.

The elemental component in each sample was obtained using energy dispersive X-ray (EDX). The EDX spectrum is taken together with the SEM shows that the alloy surface

contained Cu and Pb. According to the EDX result, it can be seen that the weight percentage (wt. %) Pb increases with the increases gradually of current density due to the increase in applied potential. The cauliflower-like conglomerates in region 'A' and 'B' (Figure 3.9) show EDX result of Cu % and Pb % ratio significantly different which brighter crystallite indicate less Pb compare darker has more Pb present. At low current density only small amount of lead is co-deposited with copper at this concentration. This structure was preserved when the amount of lead in the alloy was increased. As the cathode current density increased gradually from 4 mA cm^{-2} to 18 mA cm^{-2} the lead content of the deposit also increased from 1.54% to a higher value of approximately 20.7%. It is interesting from the EDX result that the electrodeposition of Cu-Pb alloy normally was taken place. It means, the concentration of electrodeposited element is proportional with concentration of metal in solution and the anomalous behaviour did not appear during the electrodeposition. The Pb content always below indicating normal plating with preferential deposition of Cu (the more noble metal). It is known that the increase in current density will increase the polarization of the co-deposition system. Raub stated that the factor which increased the polarization would shift the deposition ratio in favour of the less noble metal. Thus with increasing current density the proportion of the less noble metal increases during deposition. Here the cathode potential becomes more negative and hence the plating condition approached more closely to those which are represented by the current density –potential curve of the less noble metal. This condition increased the proportion of the less noble metal in the deposit. Brenner's explanation was similar. This investigation agrees with reason given by Raub and also by Brenner who explained why the Pb content increased with current density.

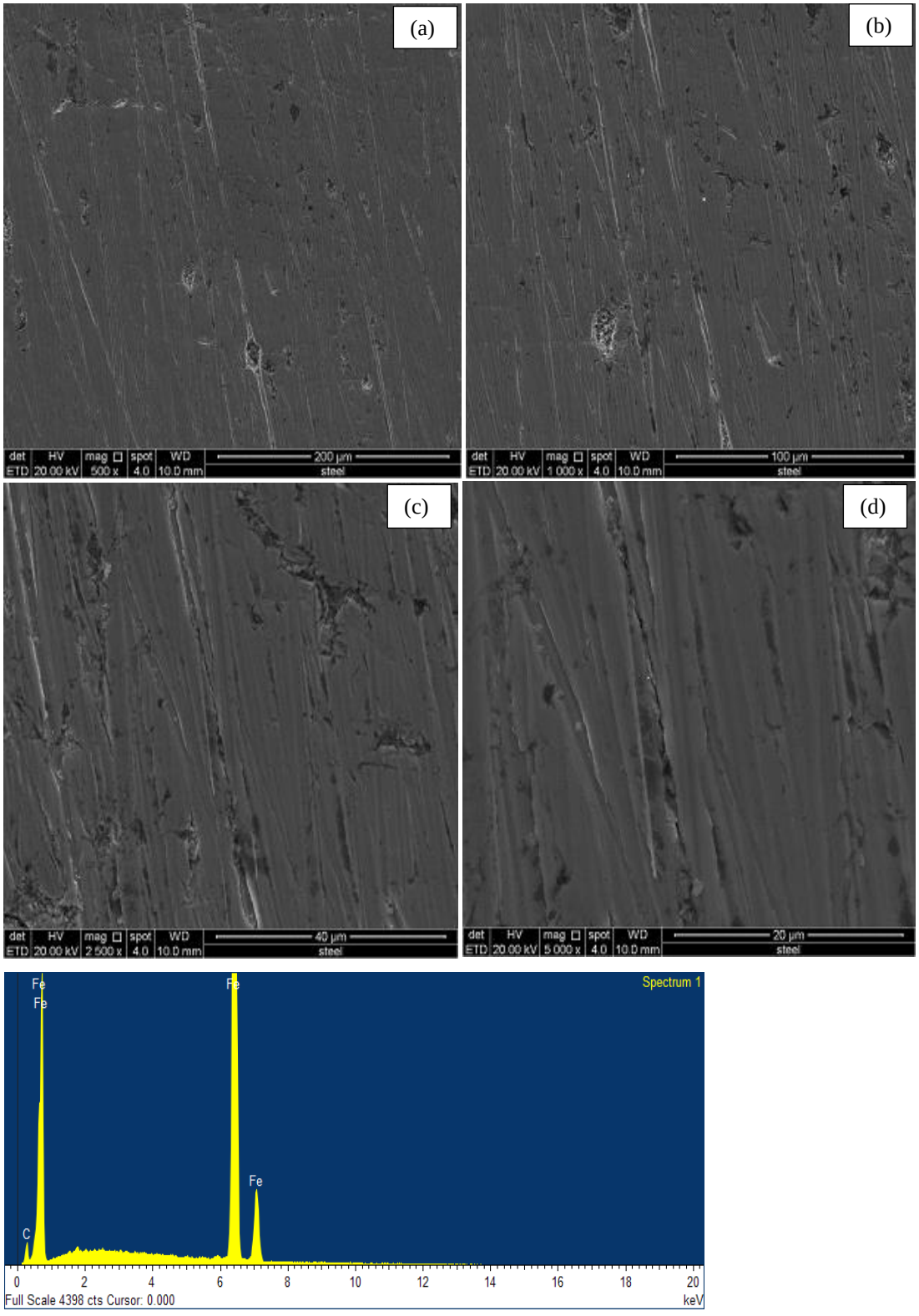

Figure 3.5: SEM micrograph of uncoated steel at different magnifications (*a*) 500, (*b*) 1000, (*c*) 2500 and (*d*) 5000 times , together with the EDX spectrum.

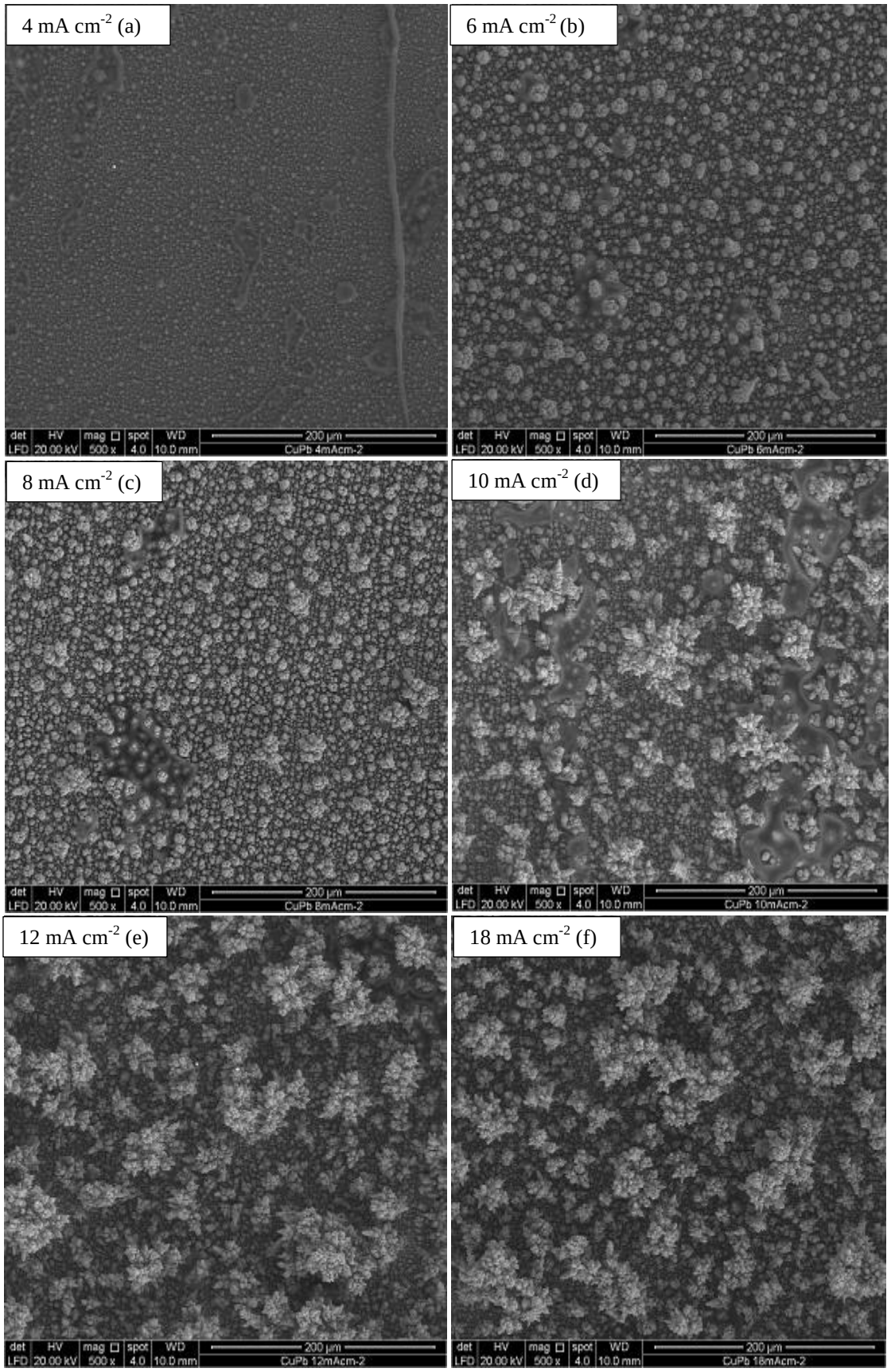

Figure 3.6 SEM Micrographs (magnification 500 times) of Cu-Pb alloy electrodeposited from MSA aqueous solution at different current densities for 45 min.

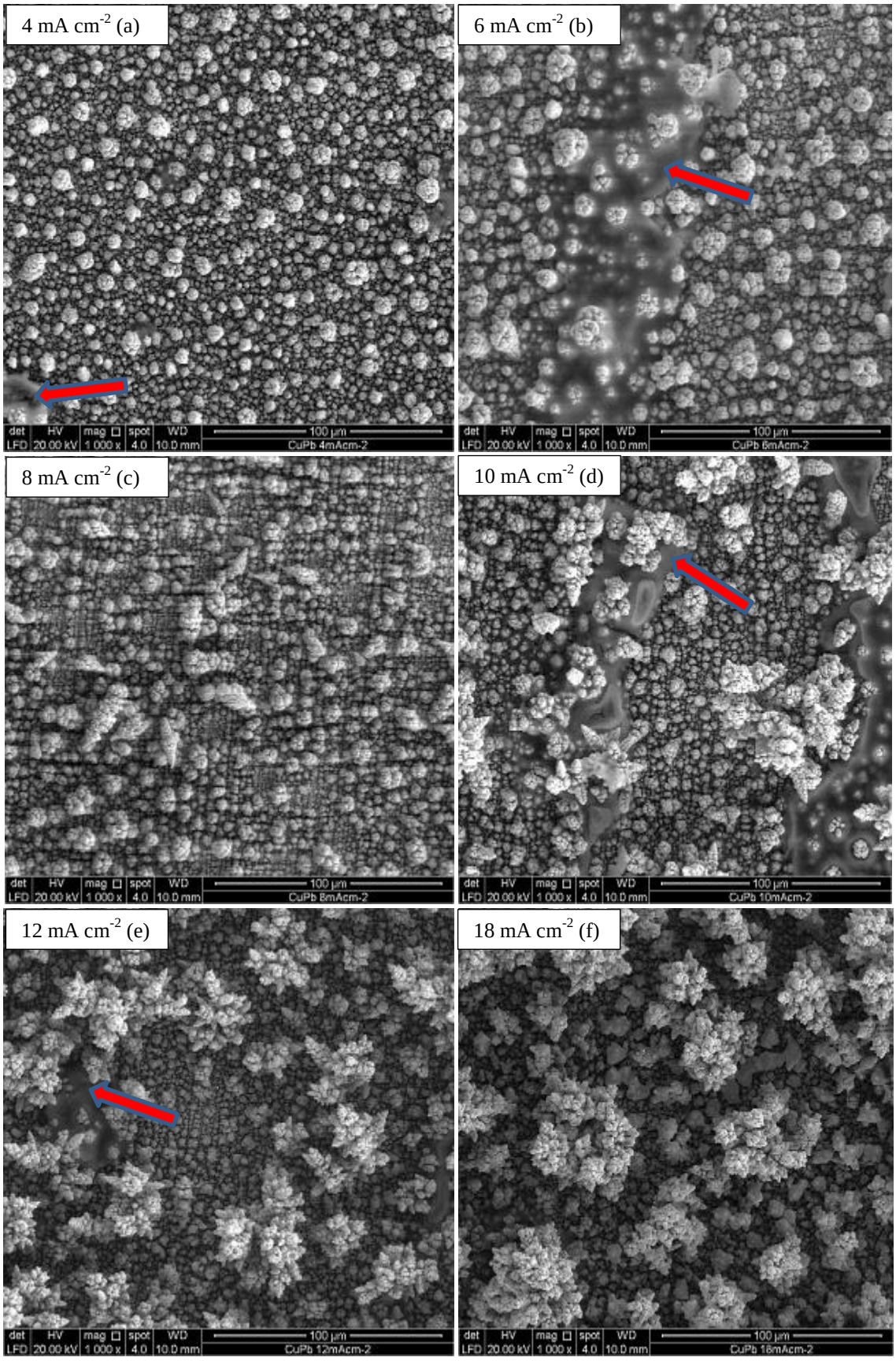

Figure 3.7 SEM Micrographs (magnification 1,000 times) of Cu-Pb alloy electrodeposited from MSA aqueous solution at a different current densities for 45 min.

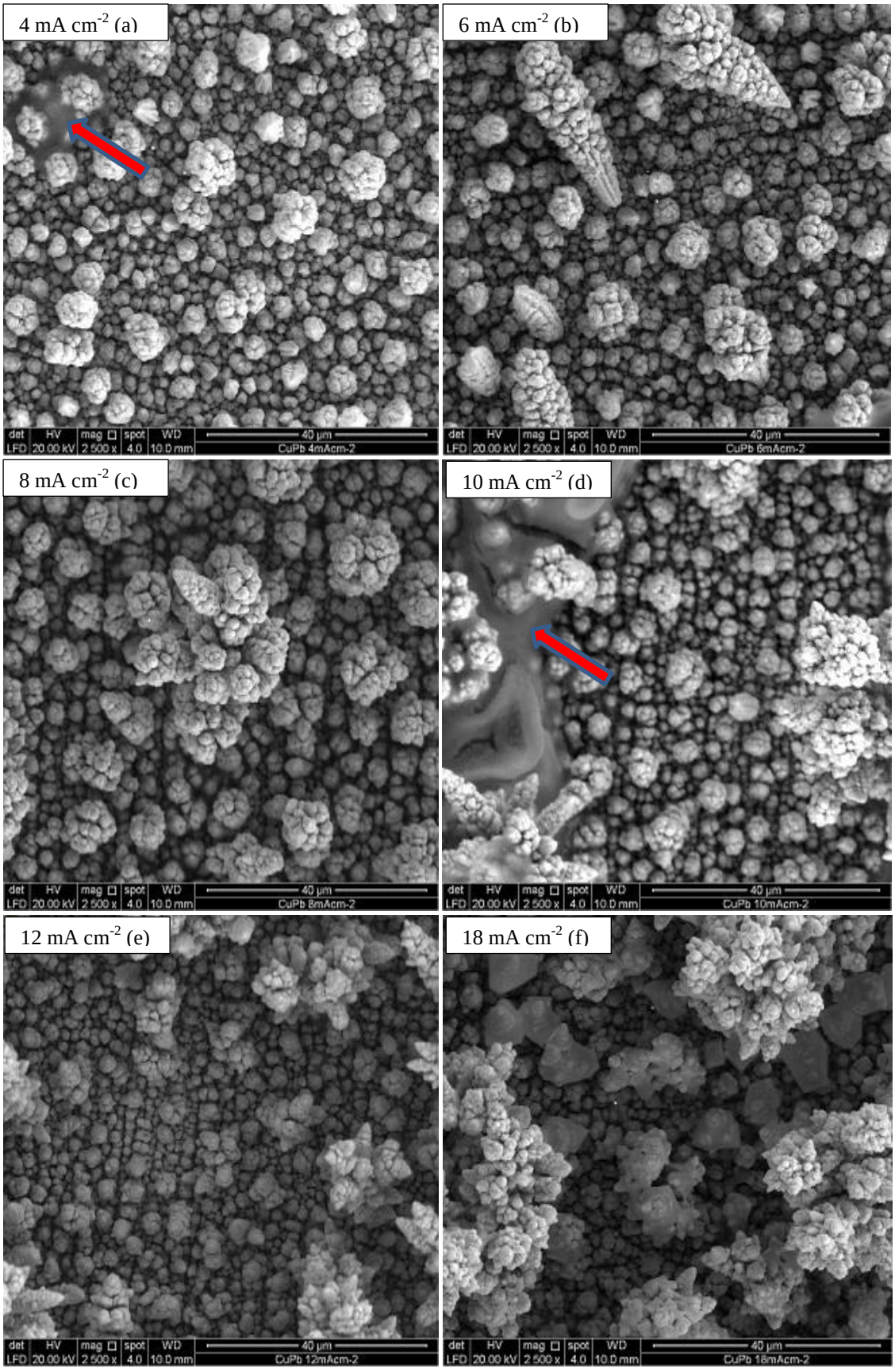

Figure 3.8 SEM micrographs (magnification 2,500 times) of Cu-Pb alloy electrodeposited from MSA aqueous solution at a different current densities for 45 min.

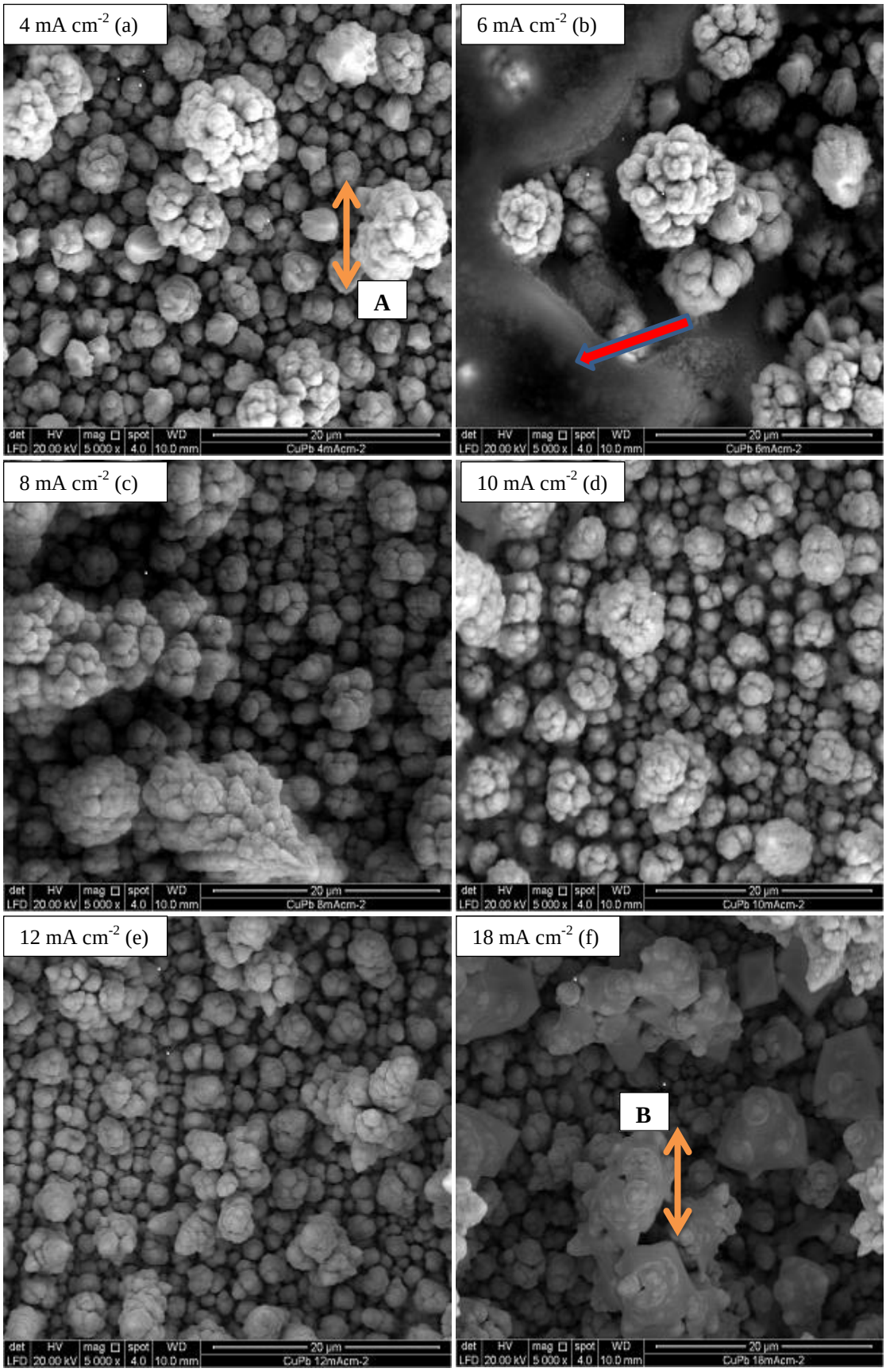

Figure 3.9: SEM micrographs (magnification 5,000 times) of Cu-Pb alloy electrodeposited from MSA aqueous solution at a different current densities for 45 min.

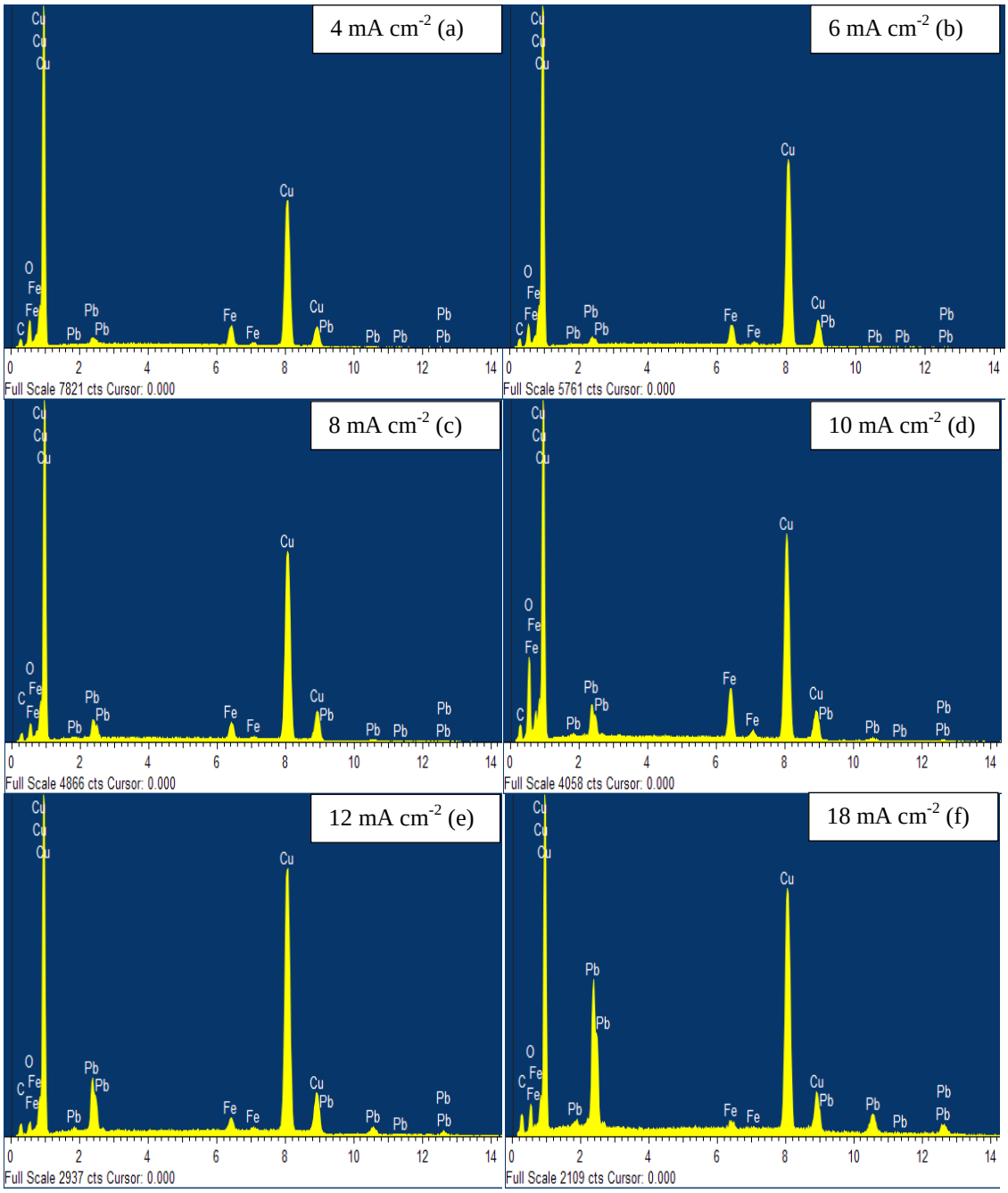

Figure 3.10: EDX spectrum to show the composition of electrodeposited Cu-Pb layer at different current density.

Table 3.7 EDX result of the percentage of elements in Cu-Pb alloy electrodeposited from MSA electrolyte at different current densities

Component → **Current Density ↓** **mA cm^{-2}**	**Cu %**	**Pb %**
4	87.60	1.54
6	85.66	1.92
8	84.85	4.33
10	80.69	6.84
12	76.98	9.66
18	68.74	20.67

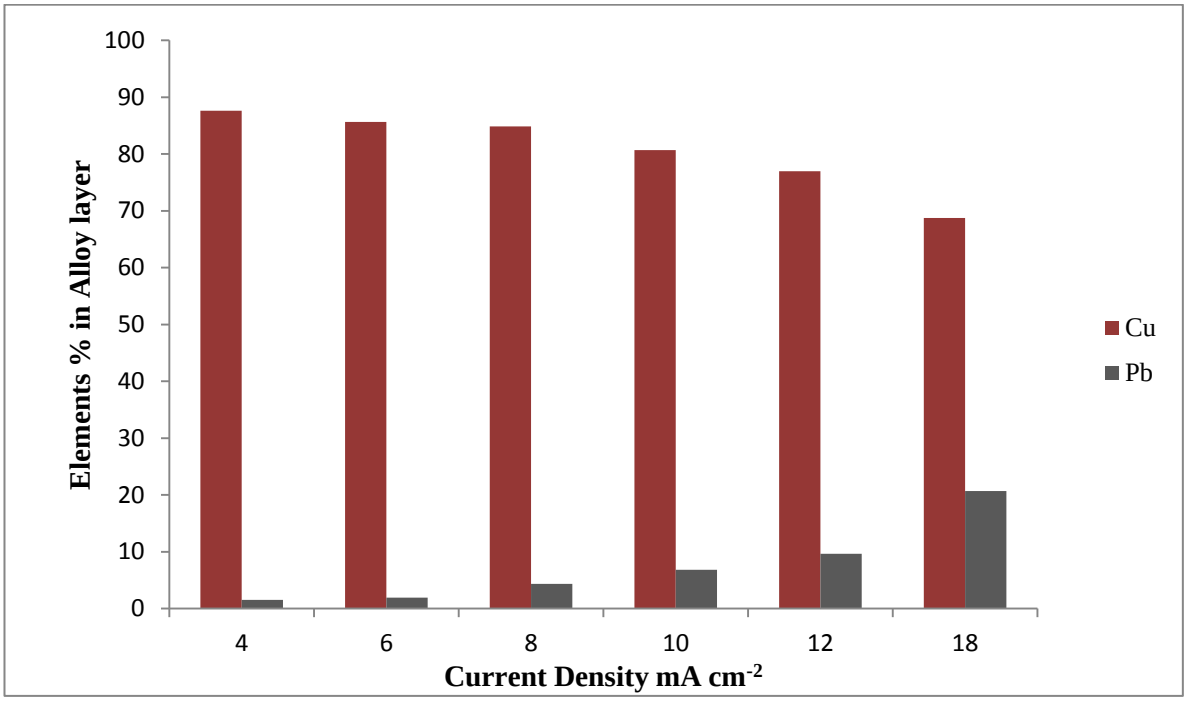

Figure 3.11 EDX result of the percentage of elements in Cu-Pb alloy electrodeposited from MSA electrolyte at different current densities

3.7 Cyclic voltammetry

This study examined the electrochemical behaviour of electrodeposition of copper, lead, and copper-lead alloys on a static steel electrode in methane sulfonate acid solution (MSA). Cyylic voltammetry (CV) was used to determine the potential at which individual metal started to deposit and when alloy co-deposited occurred. CVs were carried out using solution containing metals salts without surfactant as well as a background electrolyte containing only MSA. The pre-treatment of working electrode (Steel plates: 0.01 x 1 x 1 cm) was mentioned in the experimental method section of this project research. Types of electrodes were described in experimental section as well. The reduction potential of each metal copper and lead in its own corresponding electrolyte containing only a single metal ion was determined. These were then compared to the reduction potential observed in the electrolyte containing both metal ions to determine the potential at which Cu-Pb was being codeposited. Figure 3.12 – 3.16 shows the voltammograms of the Cu, Pb and mixture Cu-Pb in the presence of MSA. CV was forward cathodic sweep from 0 to -1.0 vs. SCE after which the scan was reversed. The potential sweep rate was remained at 25 mVs^{-1} throughout the experiments. The potential of electro-reduction decrease in the order of $Cu^{2+} > Pb^{2+}$ to more negative potentials, where the standard potential are given as +0.34 V and -0.13 V respectively.

Figure 3.12 (a) shows the cyclic voltammetry of copper electrodeposited onto a steel surface from a methanesulfonic acid electrolyte under static conditions. The electrolyte was 0.1 mol dm^{-3} $Cu(OOCCH_3)_2$ and 1 mol dm^{-3} MSA in the absence of additive. The forward cathodic sweep from 0 to – 1.0 V vs. SCE shows a single reduction peak for copper deposition corresponding to a two-electron step:

$Cu^{2+} + 2e^{-} \rightarrow Cu$ …….. (3.8)

The peak current density is associated with the complete consumption of Cu^{2+} ions at the electrode surface under mass transport control. Cu deposition current begins to flow at the potential about -0.11 V and MSA shows a strong inhibition for Cu deposition at more negative potential. On reversing the potential sweep from −1.0 to 0 V vs. SCE, a steep rise in anodic current appeared due to the oxygen evolution reaction. A curious thing happens on the reverse scan, when Cu in brown colour deposited were seen on the steel working electrode after the experiment. Even though the potential is increased to more positive scanning about 1.6 V (Figure 3.12 (b)) the copper insist strong adherent with steel and the absence of an oxidation peak Cu^0 metal to Cu^{2+} ions.

Meanwhile in Figure 3.15 shows that the CV of copper electrodeposited onto a glassy carbon electrode from a MSA electrolyte remain under static condition. The electrolyte concentration change to 0.02 mol dm^{-3} $Cu(OOCCH_3)_2$ and 2.0 mol dm^{-3} MSA without additive. The potential window examined was between -0.70 and 0.50 v vs SCE. The existence of a clear reduction and oxidation peaks was confirmed by CV experiment in MSA medium. The corresponding electrode potential shows the reduction of Cu^{2+} ions to Cu^0 metal started at approximately -0.24 V. The low current density is found in the deposition of copper. On the reverse scan only one striping peak corresponding to the oxidation of Cu^0 to Cu^{2+}.

The CV curve of the 0. 1 mol dm^{-3} $Pb(OOCCH_3)_2$ in 2.0 mol dm^{-3} MSA electrolyte is presented in Figure 3.13, it is seen that the CV curve have a double reduction peak. The most likely explanation for these features is that the reduction of water to generate hydrogen and another reduction peak potential about −0.38 V is corresponding to the reduction of Pb^{2+} ions to Pb^0 metal. Same thing happen during reverse scan from −1.0 to 0 V vs. SCE which dark grey Pb deposit were seen on the steel working electrode after the experiment. It is indicate a strong coating between lead and substrate or no oxidation occur from Pb^0 metal to Pb^{2+} ions.

However CV recorded in (Figure 3.16) for solution of 0.01 mol dm^{-3} $Pb(OOCCH_3)_2$ in 2.0 mol dm^{-3} MSA electrolyte under static conditions is totally opposite. A single reduction and oxidation peak were observed in the CV of lead deposition and dissolution on a glassy carbon electrode. It can be seen that current does not increase significantly within the potential window. The forward cathodic from 0 to -1.0 v vs SCE show the reduction peak for lead deposition corresponding to a two electron step:

$Pb^{2+} + 2e^- \rightarrow Pb$ (cathodic) ……. (3.9)

Pb deposition current begins to flow at the potential about -0.58 V. On reversing the potential sweep from -1.0 to 0 vs SCE, a single stripping sharp peak was observed confirming the two electron oxidation of metallic to lead ions via the reverse reaction:

$Pb \rightarrow Pb^{2+} + 2e^-$ (Anodic) …….. (3.10)

Cu-Pb cannot be readily co-deposited due to fact that the reduction potential of the two individual metals are far apart. This has been partially resolved by maintaining a low concentration of the more noble metal in the solution as our approach of using a Cu^{2+}: Pb^{2+} concentration of 1:3 demonstrates. This strategy has been proposed by other researcher for system such as Cu-Ni and Cu-Co, where the deposition potential of two reduction ions are separated by a large potential gap (P.Bradley, S.Roy, et al.1996).

Figure 3.14 show the CV for a solution containing both copper and lead ions. The electrolyte was 0.1 mol dm^{-3} $Cu(OOCCH_3)_2$ and 0.3 mol dm^{-3} $Pb(OOCCH_3)_2$ in 1.0 mol dm^{-3} MSA without additive. The potential was scanned from 0 to -1.0 V to cover entire range of metal deposition and dissolution. It is region both copper and lead co-deposit since these potential exceed the reduction potential of both copper and lead. However from the CV curve it's not clearly seen the two reduction peak but steel substrate show appearance Cu-Pb coated. The broadening makes it difficult to identify exact peak position. The reverse scan show the straight linear which corresponds to the Pb and Cu dissolution not take places. A dull dark grey brownish Cu-Pb co-deposit were seen on

the steel working electrode after the experiment. The similarity in electrochemical behaviour of the individual metals with that co-deposition is indicating independent alloy plating.

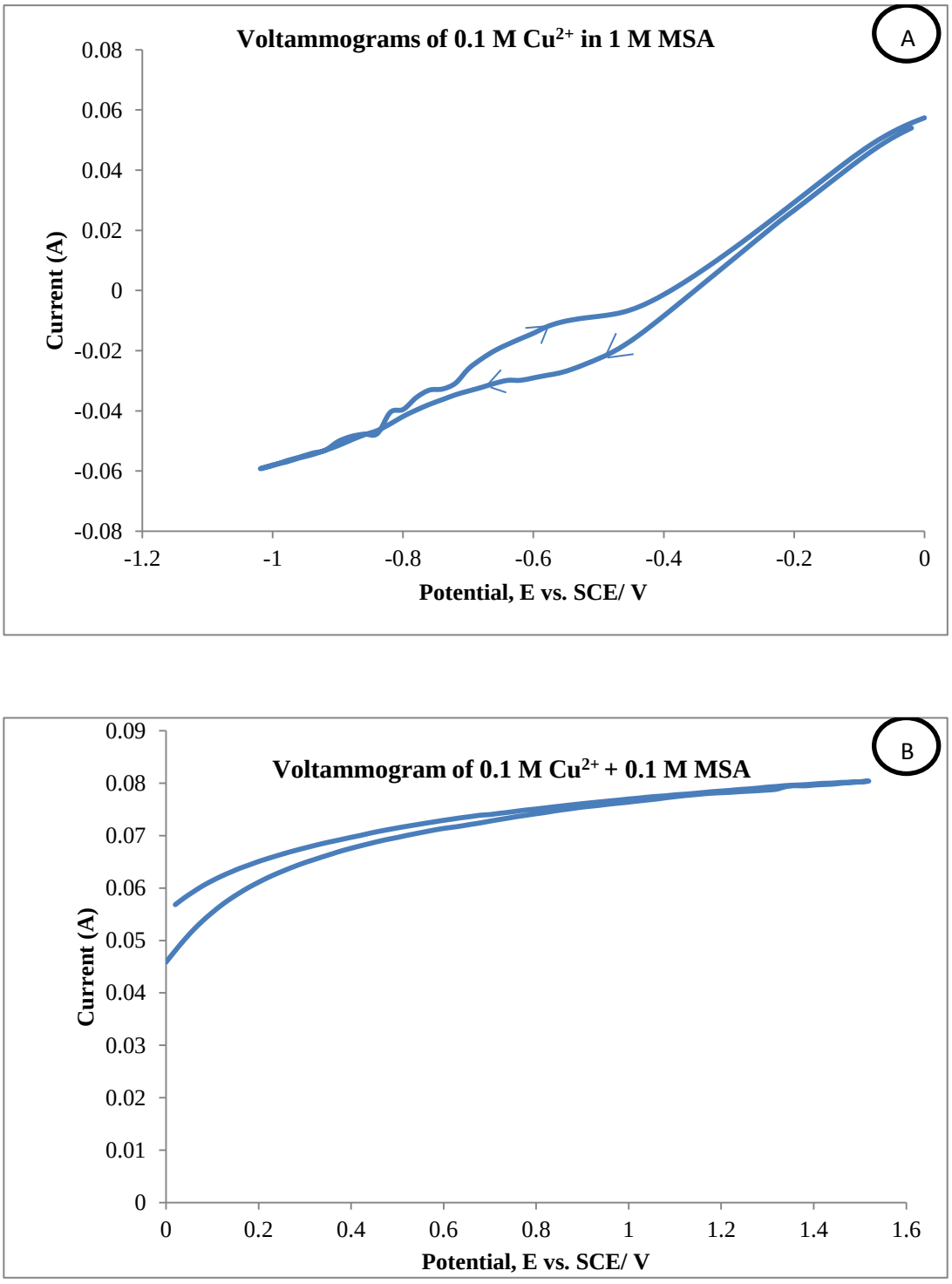

Figure 3.12 Cyclic voltammograms for steel substrate in the solution of 0.1 mol dm^{-3} Cu^{2+} + 1 mol dm^{-3} MSA. The electrodes were not stirred and the scan rate was 25 mV s^{-1}.
(A)Negative potential
(B)Positive potential

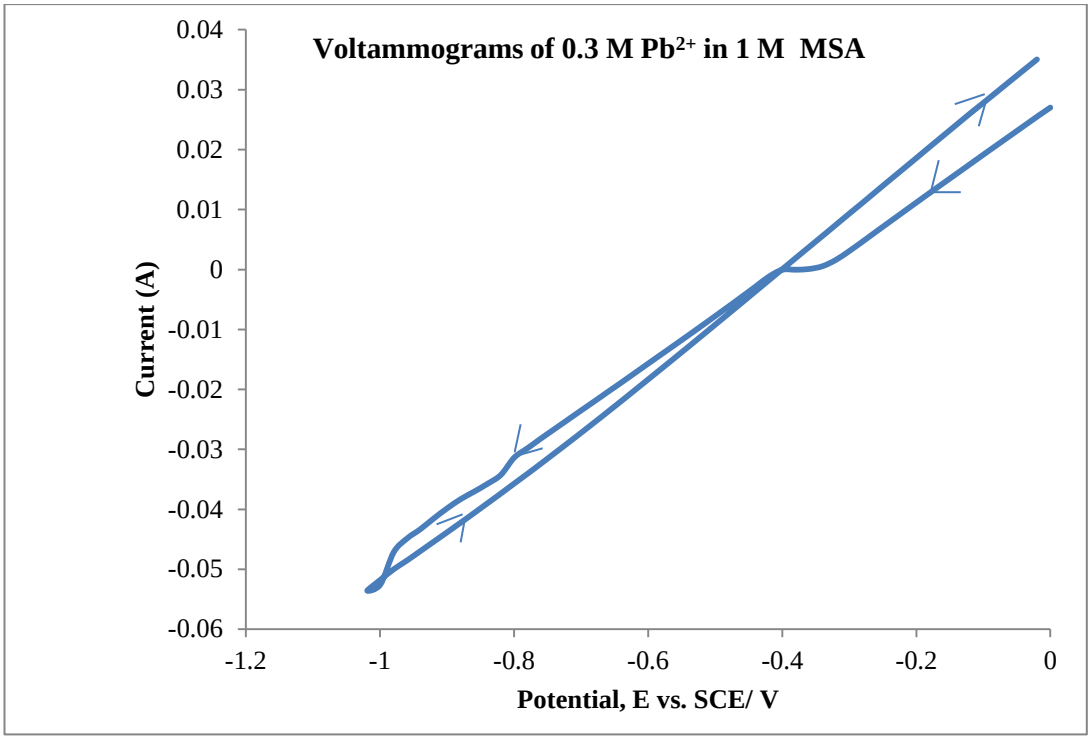

Figure 3.13 Show the cyclic voltammogram recorded for steel electrode in 0.3 mol dm^{-3} Pb^{2+} + 1 mol dm^{-3} MSA with the scan rate of 25 mV s^{-1}.

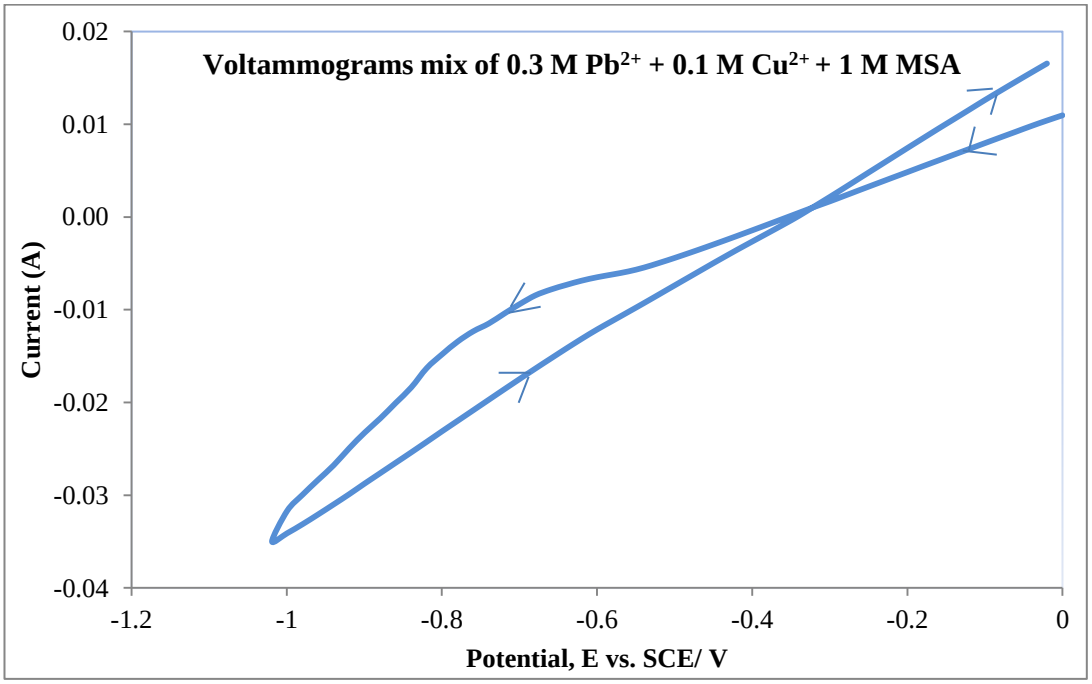

Figure 3.14 Cyclic voltammetry of copper-lead alloy on steel substrate from an electrolyte composed of 0.1 mol dm^{-3} $Cu(OOCCH_3)_2$, 0.3 mol dm^{-3} $Pb(OOCCH_3)_2$ and 1.0 mol dm^{-3} methanesulfonic acid. The electrode were not stirred and the scan rate was 25 mV s^{-1}.

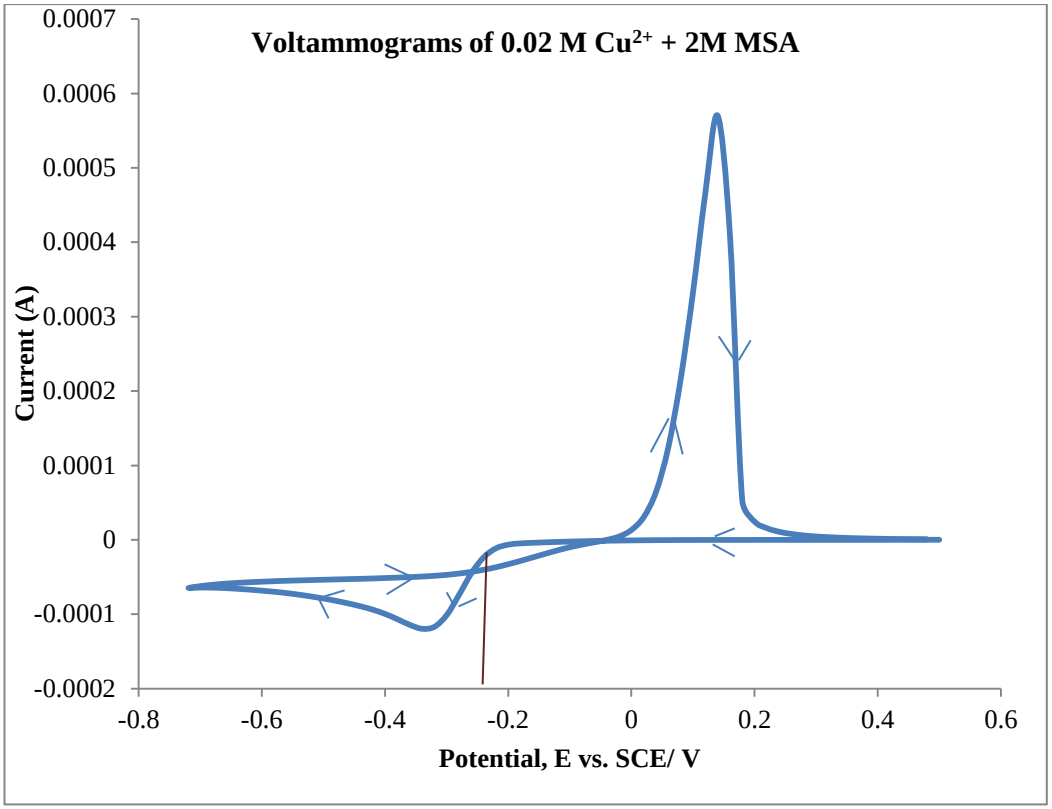

Figure 3.15: Cyclic Voltammograms of a glassy carbon electrode in solution of 0.02 mol dm^{-3} Cu^{2+} + 2 mol dm^{-3} MSA, potential sweep rate at 25 mV s^{-1}

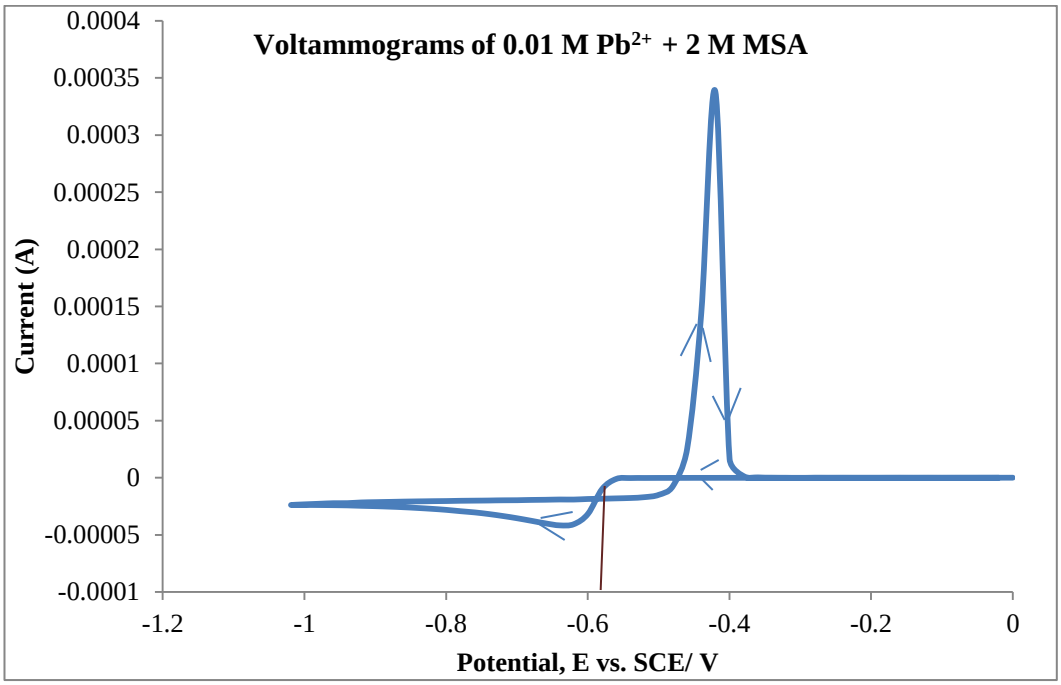

Figure 3.16: Cyclic Voltammograms of a glassy carbon electrode in solution of 0.01 mol dm^{-3} Pb^{2+} + 2 mol dm^{-3} MSA, potential sweep rate at 25 mV s^{-1}